arXiv:1401.1601v1 [astro-ph.HE] 8 Jan 2014

X-Ray Afterglow Plateaus of Long Gamma-Ray Bursts: Further Evidence for Millisecond Magnetars

S. X. Yi[1,2], Z. G. Dai[1,2], X. F. Wu[3,4,5], and F. Y. Wang[1,2]

[1]*School of Astronomy and Space Science, Nanjing University, Nanjing, China; dzg@nju.edu.cn*

[2]*Key laboratory of Modern Astronomy and Astrophysics (Nanjing University), Ministry of Education, Nanjing 210093, China*

[3]*Purple Mountain Observatory, Chinese Academy of Sciences, Nanjing 210008, China*

[4]*Chinese Center for Antarctic Astronomy, Chinese Academy of Sciences, Nanjing, 210008, China*

[5]*Joint Center for Particle Nuclear Physics and Cosmology of Purple Mountain Observatory-Nanjing University, Chinese Academy of Sciences, Nanjing 210008, China*

ABSTRACT

Many long-duration gamma-ray bursts (GRBs) were observed by *Swift*/XRT to have plateaus in their X-ray afterglow light curves. This plateau phase has been argued to be evidence for long-lasting activity of magnetar (ultra-strongly magnetized neutron stars) central engines. However, the emission efficiency of such magnetars in X-rays is still unknown. Here we collect 24 long GRB X-ray afterglows showing plateaus followed by steep decays. We extend the well-known relationship between the X-ray luminosity $L_{\rm X}$ and spin-down luminosity $L_{\rm sd}$ of pulsars to magnetar central engines, and find that the initial rotation period P_0 ranges from 1 ms to 10 ms and that the dipole magnetic field B is centered around 10^{15} G. These constraints not only favor the suggestion that the central engines of some long GRBs are very likely to be rapidly rotating magnetars but also indicate that the magnetar plateau emission efficiency in X-rays is close to 100%.

Subject headings: gamma-ray burst: general — radiation mechanisms: nonthermal — stars: pulsars

1. Introduction

Many gamma-ray bursts (GRBs) observed by *Swift*/XRT present plateaus prior to the subsequent power-law decay phase in their early X-ray afterglows (Zhang et al. 2006; Nousek et al.

2006). The plateaus generally appear in 100-1000 s since the GRB trigger with a typical slope $\alpha_1 \sim 0.5$ (Liang et al. 2007), where the flux of the plateau evolves as $F \propto t^{-\alpha_1}$. The distribution of the observed temporal decay slope α_2 (defined in $F \propto t^{-\alpha_2}$) after the plateau, ranging from less than 1 to much greater than 1 (even to 10), is quite diverse. According to the standard model for GRB afterglows (for a recent complete reference see Gao et al. (2013b)), it is hard to understand some observed α_2 with large values. Unless the plateau happens to be followed with the jet-like phase, which seems to be unlikely, the external shock models can not explain $\alpha_2 > 1.75$ (for details see next section). Therefore, it is now known that there are generally two types of plateaus. The first one is "external plateau", characterized by a normal decay ($\alpha_2 \leq 1.75$) after the plateau, which is currently understood as being due to energy injection into the external shock (Dai & Lu 1998a,b; Zhang & Mészáros 2001). A tight correlation for X-ray plateaus between the break time T_b and the corresponding X-ray luminosity $L_{\rm X}$ was recently discovered by Dainotti et al. (2010) and Xu & Huang (2012), who selected the sample with the slope of the follow-up decay phase generally less than 1.5. The second type is called "internal plateau", characterized by a steep decay ($\alpha_2 > 1.75$) after the plateau, which might be originated from internal dissipation of magnetic energy continuously blew out from the central engine (Troja et al. 2007). One possible candidate of the central engine responsible for external energy injection as well as internally dissipative magnetic energy is an ultra highly magnetized and rapidly rotating neutron star, which is also called magnetar (Thompson & Duncan 1995). The rotation energy of the magnetar can be tapped through magnetic dipole radiation (MDR) and/or relativistic leptonic wind (Dai 2004). This speculation can be realized if the initial rotation period P_0 and dipole magnetic field B of the central neutron stars are found to be consistent with our expectation (Fan & Xu 2006; Dai & Liu 2012).

Since the magnetar model is almost the only successful model for internal plateaus[1], assuming dissipative magnetic energy is from MDR, one can derive the initial period P_0 and magnetic field strength B if the spin-down luminosity $L_{\rm sd}$ and spin-down timescale $T_{\rm sd}$ of the magnetar are known. Rowlinson et al. (2013) applied this method by assuming the emission efficiency $\eta \equiv L_{\rm rad}/L_{\rm sd} = 100\%$ to fit the observed X-ray plateaus, where $L_{\rm rad}$ is the total bolometric luminosity in the $1-10^4$ keV in the cosmologically rest frame extrapolated from the observed X-ray luminosity $L_{\rm X}$ measured by *Swift*/XRT. Zhang (2009) considered five remarkable plateaus with sharp drops as a sample to discuss magnetars as the central engine of GRBs, and found that the luminosity emitted in X-ray band is a fraction of the total spin-down luminosity. In this paper, we collect all *Swift* long GRBs with a steep decay after the plateau and infer the stellar parameters based on the magnetar

[1]Matter-dominated energy injection is also possible for external plateaus, which is impulsively ejected and does not need long-lived central engine activity. It only requires a large variation in Lorentz factor. For large sample applications see Nousek et al. (2006) and Zhang et al. (2006).

model. We assume that the end time of the plateau phase corresponds to the spin-down time scale $T_{\rm sd}$ and that $\eta \lesssim 100\%$ is an adjustable parameter.

To more understand the physics behind η, we draw lessons from persistent X-ray emission of normal pulsars. The dissipation of the rotation energy of a normal pulsar to its persistent X-ray radiation could be similar to or the same as a millisecond magnetar in a GRB, in which both spin down through magnetic dipole radiation. Unlike GRB magnetars, the emission efficiency of a pulsar in X-ray can be directly calculated as the observed X-ray luminosity $L_{\rm X}$ divided by the spin-down luminosity $L_{\rm sd}$. In order to understand the mechanism by which the stellar rotation energy is converted into X-ray emission, a tight correlation between $L_{\rm X}$ and $L_{\rm sd}$ of pulsars has been widely studied (Seward & Wang 1988; Becker & Truemper 1997; Possenti et al. 2002; Cheng et al. 2004). Because distinct components of X-ray emission have different origins for normal pulsars, we here focus on the nonpulsed component of X-ray emission from pulsar wind nebulae (PWNe). As stated above, since both millisecond magnetars in GRBs and normal pulsars spin down through magnetic dipole radiation, we assume that they have the same correlation between $L_{\rm X}$ and $L_{\rm sd}$. Evidence for this assumption is as follows. (1) Gavriil et al. (2008) found that the the dipolar magnetic field of the young pulsar PSR J1846.0258 is about 4.9×10^{13} G, which is higher than those of normal pulsars, but lower than those of magnetars. Moreover, the detection of magnetar-like emission from this pulsar suggests that there is a continuum of magnetar-like activity throughout all neutron stars. (2) Vink & Bamba (2009) found that the $L_{\rm X}$-$L_{\rm sd}$ correlation of the magnetar candidate anomalous X-ray pulsar 1E1547.0-5408 is similar to that of PWN pulsars. In this paper, therefore, we extend the $L_{\rm X}$-$L_{\rm sd}$ correlation from normal pulsars to magnetars, and obtain the spin-down luminosity of magnetars by using the observed luminosity of a plateau.

The structure of the paper is as follows. In the next section, we introduce the selection of the pulsar and plateau samples, and carry out empirical fittings to the observed plateau light curves. The correlation in and between pulsars and GRBs are calculated and discussed in section 3. Our conclusions and discussion are presented in the last section.

2. Sample Selection and Light Curve Fitting

The nonthermal nonpulsed X-ray emission from rotation-powered pulsars has been studied in the context of emission from PWNe. Here we mainly investigate the nonpulsed X-ray emission from PWNe. We exclude X-ray pulsars powered by accretion from binary companions, and collect X-ray observational data of 101 pulsars with PWN from the published literature (Possenti et al. 2002; Cheng et al. 2004; Li et al. 2008; Kargaltsev & Pavlov 2010). We find a correlation of $L_{\rm X}$-$L_{\rm sd}$ with the 101 PWN sample (see next section). This correlation also indicates the fraction of the rotational energy loss of a pulsar going into X-ray emission.

X-ray plateaus are a common phenomenon in the afterglow observations. Much work has been done for theoretical explanations and statistic analysis for shallow decays (Dai & Lu 1998a,b; Zhang & Mészáros 2001; Dai 2004; Liang et al. 2007; Dai & Liu 2012; Yu & Dai 2007; Yu et al. 2010; Dainotti et al. 2010; Xu & Huang 2012). In the external shock models, usually the decay slope after the plateau is $\alpha_2 = (3p-2)/4$ if the environment is an interstellar medium (ISM) with a constant density, or sometimes (almost unlikely in X-ray after the plateau phase) $\alpha_2 = (3p-1)/4$ if the environment is a stellar wind, where p is the power-law index of the energy distribution of shock-accelerated electrons. The typical value of p is about 2.3, however, it can range from 2.0 to 3.0 or even more smaller and larger. Therefore, the typical value of α_2 is ~ 1.2 and the maximal allowable value by the model is 1.75. The possibility of the coincidence that the plateau happens to be followed by the jet-like phase is extremely small. Even in this case, $\alpha_2 = \alpha_1 + 0.75 \sim 1.3$ for an ISM environment and $\alpha_2 = \alpha_1 + 0.5 \sim 1.0$ for a wind environment, as long as the jet sideways expansion can be neglected. If the jet sideways expansion play the role, the value of $\alpha_2 = p$ is typically $2.0-3.0$. As can be seen, the above values of α_2 can not explain the large decay slope after the plateau observed in some GRBs. Internal plateaus with large α_2 are thought to be due to magnetic energy dissipation at small radii, so that when the central engine ceases the decay timescale (equivalent to decay slope) is very short. In this paper, we focus on internal plateaus and the criterion to be internal plateaus is $\alpha_2 > 1.75$. We have collected 24 long duration GRB ($T_{90} \geq 2$ s) X-ray plateaus with this judgement. Some of the GRBs in this sample have no redshift measurements, and we adopt pseudo-redshift estimated by the $L_{\rm X} - T_b$ correlation for them (Dainotti et al. 2010). We suppose that the ending of an X-ray plateau corresponds to the spin-down time of the magnetar. The centrifugal force reduces as the magnetar spins down significantly, the magnetar collapses into a black hole due to the imbalance of the gravity and outward forces[2]. It is likely that the ending of the plateau, the spin-down and collapse of the magnetar coincidently happen at the same time.

we have collected 24 remarkable X-ray afterglow light curves in our sample. We apply a smooth broken power-law and an extra power-law to fit the light curves. The fitting results are summarized in Table 1. Generally speaking, the break (ending) time ($10^4 - 10^5$ s) of internal plateaus is longer than that ($10^3 - 10^4$ s) of normal/external plateaus. The break time of the internal plateau (T_b) is assumed to be the spin-down time of a magnetar ($T_{\rm sd}$), i.e.

$$T_{\rm sd} = \frac{3c^3 I}{B^2 R^6 \Omega_0^2} = \frac{3c^3 I P_0^2}{4\pi^2 B^2 R^6}, \quad (1)$$

where $\Omega_0 = 2\pi/P_0$ is the initial angular frequency, I is moment of inertia, R is the stellar radius,

[2]Recently, Zhang (2014) applied this scenario to interpret fast radio bursts (FRBs), a new type of cosmological transients, although the physical nature is still unknown.

and c is the speed of light. The isotropic X-ray luminosity at the break time T_b is calculated by

$$L_{\rm X} = \frac{4\pi D_L^2 F_{\rm X}}{(1+z)^{1-\beta}}, \tag{2}$$

where z is the redshift, D_L is the luminosity distance, $F_{\rm X}$ is the observed X-ray flux at the end time of the plateau phase, and β is the spectral index of the X-ray afterglow which can be found from the *Swift*/XRT website (Evans et al. 2009). The spin-down luminosity of a pulsar/magnetar can be expressed as

$$L_{\rm sd} = \frac{I\,\Omega_0^2}{2\,T_{\rm sd}}, \tag{3}$$

when $t \ll T_{\rm sd}$. With equations (1) and (3), we obtain the initial period and the dipole magnetic field of the pulsar/magnetar as

$$B = \left(\frac{3c^3 I^2}{2\,R^6 L_{\rm sd} T_{\rm sd}^2}\right)^{1/2} \tag{4}$$

and

$$P_0 = \left(\frac{2\pi^2 I}{L_{\rm sd}\,T_{\rm sd}}\right)^{1/2}. \tag{5}$$

With the fitting results (see Table 1) and assuming $I = 2\times10^{45}$ g cm^2, $R = 1\times10^6$ cm, we can constrain the initial period (P_0) and the dipole magnetic field strength (B) of the pulsar/magnetar.

3. The $L_{\rm X} - L_{\rm sd}$ Correlation in Pulsars and GRBs

It has been found that $L_{\rm X}$ and $L_{\rm sd}$ in pulsars have a power-law relationship, but different authors have obtained different power-law indices (Seward & Wang 1988; Becker & Truemper 1997; Possenti et al. 2002; Cheng et al. 2004; Li et al. 2008). By analyzing observed X-ray data of 101 PWN pulsars from the published literature, we find that (see Figure 1) $L_{\rm X}$ and $L_{\rm sd}$ have a tight correlation

$$L_{\rm X} = 10^{-13.56\pm1.90} \times \left(\frac{L_{\rm sd}}{\rm erg\,s^{-1}}\right)^{1.28\pm0.05} {\rm erg\,s^{-1}}. \tag{6}$$

Thus, the corresponding conversion efficiency of the rotational energy of a pulsar into nonpulsed X-ray emission is

$$\eta = \frac{L_{\rm X}}{L_{\rm sd}} = 10^{-13.56\pm1.90} \left(\frac{L_{\rm sd}}{\rm erg\,s^{-1}}\right)^{0.28\pm0.05}, \tag{7}$$

showing that the efficiency η is dependent on the spin-down luminosity.

The conversion efficiency of the rotational energy of a magnetar into X-ray emission, in order to interpret X-ray plateaus, is unknown. Some papers, such as Rowlinson et al. (2013), generally adopted the efficiency of the rotational energy into the $1-10^4$ keV emission as 100% in their

calculations. However, their extrapolation from X-ray to $1-10^4$ keV is based on the X-ray spectral index, which may not be applicable beyond the XRT band. In this paper we consider X-ray plateaus followed by steep decays as central engine afterglows from magnetars, and assume that such magnetars and rotation-powered pulsars have the same mechanism that X-ray emission are from internal dissipation of Poynting flux. Evidence for this assumption comes from the possible fact that pulsars and magnetars may have the same L_X-L_{sd} correlation (Gavriil et al. 2008; Vink & Bamba 2009), that is, the L_X and L_{sd} of the magnetar candidate, the anomalous X-ray pulsar 1E1547.0-5408, satisfy the correlation in PWN pulsars. Therefore, we extend the correlation of L_X and L_{sd} from rotation-powered pulsars to magnetars. The corresponding conversion efficiency of the rotational energy of a magnetar into X-ray emission is also given by equation (7).

The spin-down luminosity during X-ray plateaus can be calculated by equation (6), where L_X is the luminosity at the end of the plateau (see Table 1). There are some GRBs without redshift measurement. In these cases, their redshifts can be estimated by the correlation between L_X and T_b from Dainotti et al. (2010). With the derived spin-down luminosity, we can further calculate the initial period P_0 and the dipole magnetic field strength B of a magnetar with equations (4) and (5). Table 1 shows that the derived initial spin period of the magnetars ranges from 1 to 10 ms, which is well consistent with the values expected in the magnetar formation hypothesis. The dipole magnetic field B of Table 1 is in the range of $10^{14}-10^{15}$ G, which is consistent with the magnetic field of soft gamma-ray repeaters and anomalous X-ray pulsars.

Figure 2 shows the magnetic field and spin period for both long and short GRB candidates. The magnetars could be roughly divided by $B = 5\times10^{15}$ G into two different samples, short GRB candidates above the line and long GRB candidates below the line. One caveat is that there are some GRBs with extended emission included in the sample plotting Figure 2. Because their distribution is similar to that of the short ones (Rowlinson et al. 2013; Gompertz et al. 2013), we consider them as one subset of the short GRB candidates. Compared with the long GRBs, the short GRB candidates tend to have higher magnetic fields. From our statistics, we find the initial spin period mainly in the range $1-10$ ms and the dipole magnetic field in the range $5\times10^{14}-5\times10^{15}$ G for the long GRB magnetars. These values are all reasonable, implying that internal plateaus could be powered by a central spinning-down magnetar.

4. Conclusions and Discussion

The X-ray plateaus can be explained as being due to continuous energy injection from central engines after the prompt bursts and rapidly rotating, ultra-strongly magnetized pulsars are good candidates of such GRB central engines. In this paper, we have collected 24 remarkable long-GRB X-ray plateaus followed by sharp drops. We assumed that the X-ray plateaus are powered

by internal magnetic energy dissipation of Poynting flux from a magnetar and the sudden drop is caused by the spin-down and collapse of the magnetar. On the other hand, we gathered the X-ray observational data on $L_{\rm X}$ and $L_{\rm sd}$ of 101 PWN pulsars from the published literature, and fitted them with a power law function (Figure 1), $L_{\rm X} = 10^{(-13.56\pm1.90)}(L_{\rm sd}/{\rm erg\,s^{-1}})^{(1.28\pm0.05)}\,{\rm erg\,s^{-1}}$. We assumed that magnetars and rotation-powered pulsars may experience a common internal dissipation mechanism. Thus, we extended the correlation of $L_{\rm X}$ and $L_{\rm sd}$ from rotation-powered pulsars to X-ray plateaus. We find that for the magnetar candidates in the 24 long GRBs, the initial period P_0 is about 1 to 10 ms, while the dipole magnetic field strength B is in the range of 10^{14} to 10^{15} G. This result implies that the central engines of some long GRBs are millisecond magnetars.

Millisecond magnetars are not only proposed as the central engines of some long GRBs, but also they may survive from some binary neutron star mergers that power short GRBs. The long-lasting activity of the central magnetars have been suggested to interpret the X-ray flares and plateaus following some short GRBs (Dai et al. 2006; Fan & Xu 2006; Rowlinson et al. 2010; Rowlinson et al. 2013) and the statistical properties of X-ray flares from both long and short GRBs (Wang & Dai 2013). Recently, such a survived massive millisecond magnetar scenario has been studied to predict a bright multi-wavelength afterglow (Gao et al. 2013a) and invoked to explain an unusual energetic transient PTF11agg (Wang & Dai 2013; Wu et al. 2014). We therefore suggest that millisecond magnetars play an important role in both long and short GRBs.

Acknowledgements

We acknowledge the use of the public data from the *Swift* archives and the data supplied by the UK *Swift* Science Data Centre at the University of Leicester. We thank Bing Zhang, Xiang-Yu Wang, Yong-Feng Huang, Wei Wang, Xuan Ding and Ling-Jun Wang for useful comments and helps. This work is supported by the National Basic Research Program of China (973 Program, grants 2014CB845800 and 2013CB834900) and the National Natural Science Foundation of China (grants 11373022, 11322328, 11103007, and 11033002). XFW acknowledges support by the One-Hundred-Talents Program and the Youth Innovation Promotion Association of Chinese Academy of Sciences.

REFERENCES

Becker, W., & Truemper, J. 1997, A&A, 326, 682

Bernardini, M. G., Margutti, R., Mao, J., Zaninoni, E., & Chincarini, G. 2012, A&A, 539, A3

Cheng, K. S., Taam, R. E., & Wang, W. 2004, ApJ, 617, 480

Cucchiara, A., Fox, D. B., Cenko, S. B., & Berger, E. 2008, GRB Coordinates Network, 8448, 1

Dai, Z. G. 2004, ApJ, 606, 1000

Dai, Z.G., Wang, X.Y., Wu, X.F., & Zhang, B. 2006, Science, 311, 1127

Dai, Z. G., & Liu, R.-Y. 2012, ApJ, 759, 58

Dai, Z. G., & Lu, T. 1998a, Physical Review Letters, 81, 4301

Dai, Z. G., & Lu, T. 1998b, A&A, 333, L87

Dainotti, M. G., Willingale, R., Capozziello, S., Fabrizio Cardone, V., & Ostrowski, M. 2010, ApJ, 722, L215

Dall'Osso, S., Stratta, G., Guetta, D., et al. 2011, A&A, 526, A121

Evans, P. A., Beardmore, A. P., Page, K. L., et al. 2009, MNRAS, 397, 1177

Fan, Y.-Z., & Xu, D. 2006, MNRAS, 372, L19

Ferrero, P., Klose, S., Kann, D. A., et al. 2009, A&A, 497, 729

Fugazza, D., Thoene, C. C., D'Elia, V., et al. 2009, GRB Coordinates Network, 8892, 1

Gao, H., Ding, X., Wu, X.F., Zhang, B., & Dai, Z.G. 2013a, ApJ, 771, 86

Gao, H., Lei, W. H., Zou, Y. C., Wu, X.F., & Zhang, B. 2013b, NewAR, 57, 141

Gavriil, F. P., et al., 2008, Science, 319, 1802

Gompertz, B. P., O'Brien, P. T., Wynn, G. A., & Rowlinson, A. 2013, MNRAS, 431, 1745

Groot, P., Kaper, L., Ellerbroek, L., et al. 2010, GRB Coordinates Network, 10441, 1

Jaunsen, A. O., Malesani, D., Fynbo, J. P. U., Sollerman, J., & Vreeswijk, P. M. 2007, GRB Coordinates Network, 6010, 1

Kargaltsev, O., & Pavlov, G. G. 2010, X-ray Astronomy 2009; Present Status, Multi-Wavelength Approach and Future Perspectives, 1248, 25

Li, X.-H., Lu, F.-J., & Li, Z. 2008, ApJ, 682, 1166

Liang, E.-W., Zhang, B.-B., & Zhang, B. 2007, ApJ, 670, 565

Lyons, N., O'Brien, P. T., Zhang, B., et al. 2010, MNRAS, 402, 705

Malesani, D., Jakobsson, P., Fynbo, J. P. U., Hjorth, J., & Vreeswijk, P. M. 2007, GRB Coordinates Network, 6651, 1

Molinari, E., Vergani, S. D., Malesani, D., et al. 2007, A&A, 469, L13

Nousek, J. A., Kouveliotou, C., Grupe, D., et al. 2006, ApJ, 642, 389

Possenti, A., Cerutti, R., Colpi, M., & Mereghetti, S. 2002, A&A, 387, 993

Rowlinson, A., O'Brien, P. T., Metzger, B. D., Tanvir, N. R., & Levan, A. J. 2013, MNRAS, 430, 1061

Rowlinson, A., O'Brien, P. T., Tanvir, N.R., et al. 2010, MNRAS, 409, 531

Seward, F. D., & Wang, Z.-R. 1988, ApJ, 332, 199

Tanvir, N. R., Wiersema, K., & Levan, A. J. 2010, GRB Coordinates Network, 11230, 1

Tanvir, N. R., Wiersema, K., Levan, A. J., et al. 2012, GRB Coordinates Network, 13348, 1

Tello, J. C., Sanchez-Ramirez, R., Gorosabel, J., et al. 2012, GRB Coordinates Network, 13118, 1

Thoene, C. C., Jakobsson, P., Fynbo, J. P. U., et al. 2007, GRB Coordinates Network, 6499, 1

Thompson, C., & Duncan, R. C. 1995, MNRAS, 275, 255

Troja, E., Cusumano, G., O'Brien, P. T., et al. 2007, ApJ, 665, 599

Vink, J. & Bamba, A., 2009, ApJ, 707, L148

Vreeswijk, P., Fynbo, J., & Melandri, A. 2011, GRB Coordinates Network, 12648, 1

Wang, F. Y., & Dai, Z. G. 2013, Nature Physics, 9, 465

Wang, L. J., & Dai, Z. G. 2013, ApJL, 774, L33

Wu, X. F., Gao, H., Ding, X., Zhnag, B., Dai, Z. G., & Wei, J. Y. 2014, ApJL, 781, L10

Xu, M., & Huang, Y. F. 2012, A&A, 538, A134

Yu, Y. W., & Dai, Z. G. 2007, A&A, 470, 119

Yu, Y.-W., Cheng, K. S., & Cao, X.-F. 2010, ApJ, 715, 477

Zhang, B., Fan, Y. Z., Dyks, J., et al. 2006, ApJ, 642, 354

Zhang, B., & Mészáros, P. 2001, ApJ, 552, L35

Zhang, B. 2014, ApJ, 780, L21

Zhang, X.-H. 2009, Research in Astronomy and Astrophysics, 9, 213

This preprint was prepared with the AAS LaTeX macros v5.2.

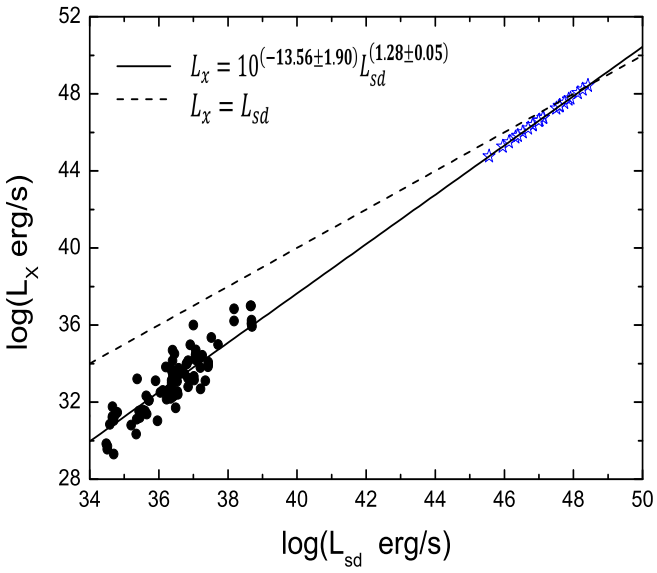

Fig. 1.— The $L_{\rm X} - L_{\rm sd}$ correlation in pulsars (solid black dots) and long GRBs (open blue stars). The solid line corresponds to the best fit for pulsars, while the dashed line is $L_{\rm sd} = L_{\rm X}$. Luminosities are in units of erg s^{-1}.

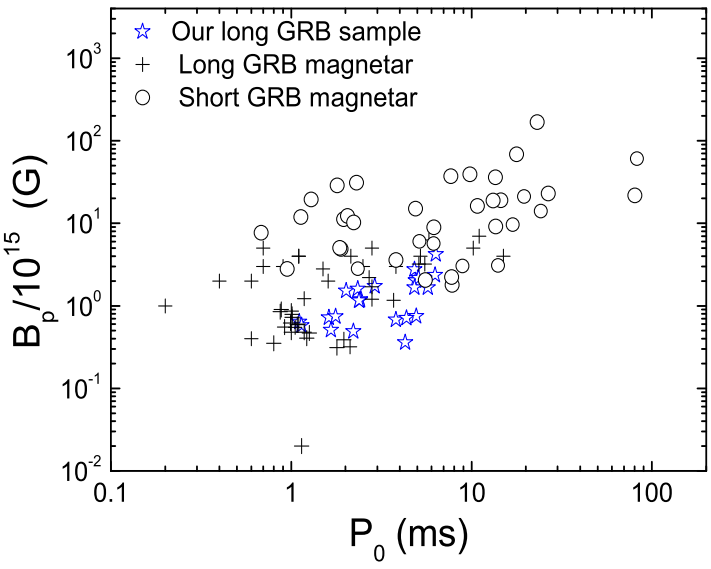

Fig. 2.— Magnetic field and spin period of the magnetar candidates in GRBs. Black crosses are the magnetar candidates in long GRBs taken from Yu et al. (2010), Lyons et al. (2010), Dall'Osso et al. (2011), Bernardini et al. (2012). Open circles are the magnetar candidates in short GRBs identified by Rowlinson et al. (2013), Gompertz et al. (2013). Open blue stars stand for our sample. Magnetars in short GRBs tend to have higher magnetic fields.

Table 1. Fitting results of X-ray plateaus and derived parameter values for magnetar candidates

GRB	z	α_1	α_2	T_b[a]	F_x[b]	L_x[c]	L_{sd}[c]	P_0[d]	B[e]	Refs.
060413	0.61*	2.2E-4 ± 0.04	3.09 ± 0.09	24224.7 ± 456.7	22.37 ± 0.65	2.35 ± 0.07	6.62	4.96	2.04	...
060605	3.8	0.42 ± 0.05	1.89 ± 0.05	7254.9 ± 252.6	8.07 ± 0.31	110.17 ± 4.30	133.85	2.02	1.52	1
060607A	3.082	0.31 ± 0.03	3.60 ± 0.07	12258.8 ± 190.4	56.24 ± 1.76	260.60 ± 8.14	262.26	1.11	0.64	2
060923C	1*	0.46 ± 0.06	1.79 ± 0.23	179436.3 ± 19430.2	0.24 ± 0.03	0.18 ± 0.03	0.90	4.94	0.75	...
070110	2.352	0.18 ± 0.05	9.79 ± 0.55	20714.4 ± 218.7	10.94 ± 0.43	50.65 ± 2.00	72.94	1.62	0.72	3
070429A	1.3*	0.34 ± 0.04	8.87 ± 4.73	592515.7 ± 67316.5	0.07 ± 0.01	0.06 ± 0.01	0.36	4.28	0.36	...
070611	2.04	-0.77 ± 0.52	1.78 ± 0.18	29274.8 ± 4800.6	0.43 ± 0.07	1.01 ± 0.16	3.42	6.27	2.35	4
070721B	3.626	0.65 ± 0.04	2.32 ± 0.10	8819.7 ± 244.1	10.18 ± 0.38	58.64 ± 2.17	81.78	2.34	1.60	5
071118	1.24*	0.39 ± 0.08	2.51 ± 0.29	12500.3 ± 478.1	9.27 ± 0.44	5.90 ± 0.28	13.60	4.82	2.76	...
080703	1.5*	0.58 ± 0.02	2.60 ± 0.20	24295.5 ± 1989.6	2.72 ± 0.55	2.41 ± 0.49	6.76	4.90	2.02	...
081029	3.848	0.42 ± 0.06	2.44 ± 0.11	16791.8 ± 1219.5	5.21 ± 0.10	23.77 ± 2.48	40.39	2.41	1.19	6
090205	4.7	0.52 ± 0.11	2.11 ± 0.19	17493.8 ± 1251.4	0.98 ± 0.08	22.60 ± 1.96	38.83	2.41	1.17	7
090308	2.38*	0.34 ± 0.36	2.94 ± 0.21	128650.9 ± 100000.0	0.06 ± 0.02	0.54 ± 0.21	2.11	3.81	0.68	...
090807	1.44*	-0.08 ± 0.07	1.79 ± 0.10	9368.0 ± 669.0	2.47 ± 0.17	4.22 ± 0.29	10.46	6.34	4.20	...
100219A	4.5	0.18 ± 0.15	2.17 ± 0.33	23527.5 ± 2365.4	3.45 ± 0.37	34.48 ± 3.68	54.01	1.76	0.74	8
100508A	1.24*	0.29 ± 0.07	2.61 ± 0.12	22563.7 ± 1055.9	4.43 ± 0.27	2.42 ± 0.15	6.77	5.08	2.17	...
100614A	1.21*	0.28 ± 0.06	2.11 ± 0.22	153270.0 ± 12469.8	0.40 ± 0.03	0.31 ± 0.02	1.36	4.36	0.71	...
100906A	1.727	0.70 ± 0.02	2.07 ± 0.04	11697.4 ± 260.2	11.52 ± 0.35	23.26 ± 0.71	39.71	2.91	1.73	9
111022B	2.5*	-0.04 ± 0.15	2.65 ± 0.70	48625.1 ± 8148.5	0.23 ± 0.04	0.67 ± 0.11	2.47	5.73	1.66	...
111209A	0.677	0.58 ± 0.00	5.47 ± 0.04	16116.0 ± 33.4	958.78 ± 5.19	169.02 ± 0.91	186.99	1.14	0.58	10
120320A	3.14*	0.02 ± 0.09	4.25 ± 0.60	82527.1 ± 8089.4	0.39 ± 0.06	3.89 ± 0.58	9.82	2.21	0.49	...
120326A	1.798	-0.38 ± 0.03	1.86 ± 0.05	44331.0 ± 1254.1	9.47 ± 0.21	17.74 ± 0.40	32.14	1.66	0.51	11
120521C	6	0.21 ± 0.11	2.12 ± 0.26	17204.3 ± 2589.3	0.84 ± 0.11	23.74 ± 3.18	40.35	2.38	1.16	12
130315A	2.04*	0.07 ± 0.12	2.41 ± 0.30	34498.6 ± 3733.4	0.60 ± 0.07	1.60 ± 0.19	4.91	4.83	1.66	...

*The redshifts of those GRBs are constrained by the correlation of L_x and T_b from Dainotti et al. (2010).

[a]In units of second.

[b]In units of 10^{-12} erg cm^{-2}s^{-1}.

[c]In units of 10^{46} erg/s.

[d]In units of ms.

[e]In units of 10^{15} G.

References. — (1) Ferrero et al. (2009); (2) Molinari et al. (2007); (3) Jaunsen et al. (2007); (4) Thoene et al. (2007); (5) Malesani et al. (2007); (6) Cucchiara et al. (2008); (7) Fugazza et al. (2009); (8) Groot et al. (2010); (9) Tanvir et al. (2010); (10) Vreeswijk et al. (2011); (11) Tello et al. (2012); (12) Tanvir et al. (2012);